

## Deterioration of the Corrosion Resistance of Welded Joints in API5L X52 Steel Isothermally Aged

B. Vargas-Arista<sup>1,\*</sup>, J. Solis Romero<sup>1</sup>, C. Angeles-Chavez<sup>2</sup>, A. Albiter<sup>2</sup>, J. M. Hallen<sup>3</sup>

<sup>1</sup> Instituto Tecnológico de Tlalnepantla, Av. Instituto Tecnológico s/n, Col. La Comunidad, Tlalnepantla de Baz, Estado de Mexico, Mexico 54070, Tel.: +52 55 55 65 32 61 Ext. 121, Fax: +52 55 53 90 03 10 Ext. 103, [www.ittla.edu.mx](http://www.ittla.edu.mx)

<sup>2</sup> Instituto Mexicano del Petróleo, Eje Central Lázaro Cárdenas Norte 152, San Bartolo Atepehuacan, México D. F. 07730

<sup>3</sup> Departamento de Ingeniería Metalúrgica, IPN-ESIQIE, Laboratorios Pesados de Metalurgia, UPALM Zacatenco, México, D. F. 07738

\*E-mail: [bvarista26@yahoo.com.mx](mailto:bvarista26@yahoo.com.mx),

*Received:* 4 November 2010 / *Accepted:* 1 December 2010 / *Published:* 1 February 2011

---

Corrosion behavior of welded joints in API5L-X52 pipe steel aged at 250 °C at different times was investigated under electrochemical technique like tafel polarization, scanning electron microscopy (SEM) and transmission electron microscopy (TEM) studies. The electrochemical results which were performed in a solution of brine containing hydrogen sulfide at 25 °C, revealed an increase of the general corrosion rate in the weld bead, the heat affected zone and the base metal as the aging time was elapsed. The corrosion rate higher was linked to the transgranular precipitation of fine nanoparticles of cementite and niobium carbide occurred during accelerated aging process until 500 hours and their coarsening process after this time. The SEM study of the corrosion products at the three different zones showed the presence of oxide and sulphur of iron very brittle and porous on metallic surface. The highest corrosion rate was reached by the weld bead owing to the largest increase in the amount of nanocarbides, lesser coarsening and the presence of corroding products with larger brittleness and porosity.

---

**Keywords:** H<sub>2</sub>S corrosion, Welded joint, Aging, API5L-X52 Steel, nanocarbides.

### 1. INTRODUCTION

The API-5L pipe steel is regularly built up with a longitudinal welding, which is performed using a submerged arc welding process. It is frequently used for oil and gas transport in the petroleum industry. This type of steel is microalloyed with chemical elements as titanium, niobium and vanadium

and it is manufactured using a thermomechanically controlled rolling process (TMCP) to control the precipitation strengthening from precipitates of Nb carbonitride during rolling, cooling and coiling [1].

On the other hand, during the operation for long period of time, the pipe steel go experimenting a natural aging which is accelerated by the service conditions such as temperature that operate a range from 25 °C to 70 °C and also variations of the working pressure. These conditions affect the mechanical properties, by changes on the microstructure as was evidenced by the artificial aging of carbon steel performed from 100 °C to 350 °C, to accelerate the effects of the natural aging [2]. The aging process has been described by a peak-aging and over-aging conditions, which have been well characterized and published elsewhere [3,4].

Is very well known that the pipeline steel surface is strongly affected by aggressive chemical components such as hydrogen sulfide (H<sub>2</sub>S), carbon dioxide (CO<sub>2</sub>) [5] and chloride ions (Cl<sup>-</sup>) that are mixed with the hydrocarbons when the pipeline transport crude oils. Generally, an aqueous solutions of brine is separated during the transport having chemical impurities as H<sub>2</sub>S, CO<sub>2</sub> and Cl<sup>-</sup> giving to the solution a pH that affect the metallic surface producing a surface deterioration by chemical corrosion in their service temperature range (25 °C to 90 °C). The H<sub>2</sub>S content can range from few ppm to > 35 % or more, is a critical variable affecting the environment assisted cracking susceptibility of weldments on API X52 steel [6].

In order to enhance the understanding about the relationship between aging and corrosion processes, several studies on aging had been reported in literature [7-10]. A previously reported results of studies on weld bead of 308 stainless steel aged at 500 °C for 24 hours, suggest that intergranular corrosion susceptibility may increase due to the chromium carbide precipitation [8]. For API-5L linepipe steel artificially aged at 250 °C, report greater susceptibility to corrosion in aqueous chloride media as a function of aging time [9]. There is a case where 2101 stainless steel aged at 700 °C during 240 minutes, shows changes in the microstructure such as the formation of small amount of precipitates, which lower its corrosion resistance [10]. However, from all the above investigations, it is not quite elucidated the relationship between the aging, microstructure and corrosion behavior for the complete heat affected zone (HAZ) and weld bead produced by the welding cycle.

Most of the line pipe used for transport of hydrocarbons having more than 20 years of service under corroding environments, is manufactured with low strength steel, which it is susceptible to aging at 250 °C [11]. Since aging phenomenon has been well characterized [3,4,12,13], it is important to study the corrosion process under the effects of the aging. Therefore, in order to accelerate the natural aging by heat treatment at 250 °C for different times and to expand the understanding of the long-term changes of natural aging in the presence of internal corrosion in a sour environment with H<sub>2</sub>S, this study was carried out.

The present work aims at investigating the effect of the accelerated aging at 250 °C for different times on the corrosion resistance, in synthetic brine with artificial hydrogen sulfide, of welded joints on the pipe steel. This approach will allow establishing the metallurgical bases to understand the corrosion behavior of the pipe naturally aged that is reaching the end of the useful life, taking into account the chemical composition of the transported fluid, which has a remarkable effect for the microstructure and mechanical properties.

## 2. EXPERIMENTAL PART

### 2.1. Material

Specimens of welded joints were obtained from a 914 mm nominal diameter API5L X52 line pipe steel welded longitudinally by double-pass DSAW through an X-groove configuration (Figure 1a), under API 1104 welding procedure specification (WPS) [14]. Table 1 shows the chemical composition of the weld bead and base metal in the untreated condition, in accordance with API 5L [15].

**Table 1.** Chemical composition of the weld bead and base metal (% by weight)

Material	Element							
	C	Mn	Si	Nb	Ti	V	P	S
Weld bead	0.046	1.14	0.27	0.050	0.020	0.030	0.021	0.010
Base metal	0.080	1.06	0.26	0.041	0.003	0.054	0.019	0.003

Square transversal electrodes (surface area = 1 cm<sup>2</sup>) were completely made from the weld bead, the HAZ and the base metal, see Figure 1a.

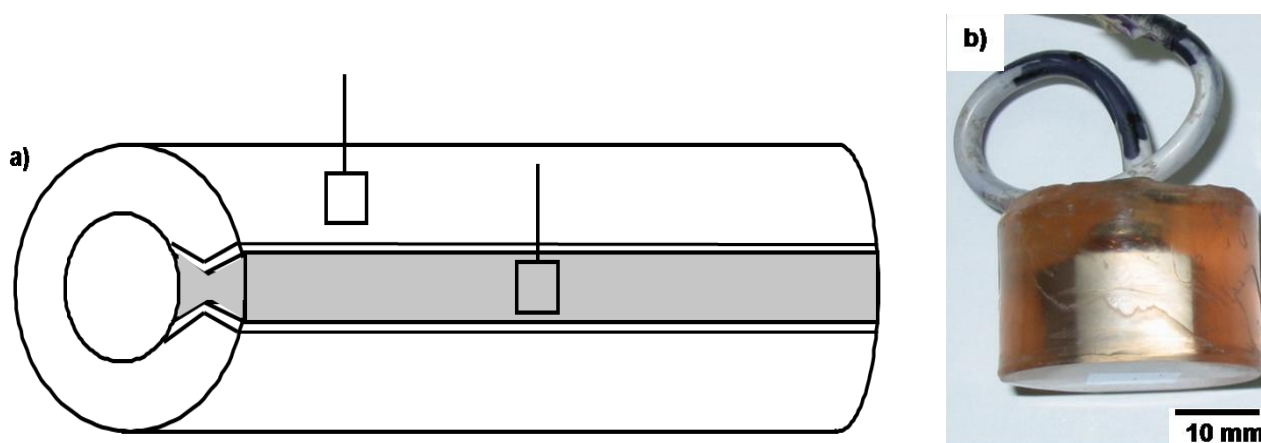


**Figure 1.** (a) schematic representation of the specimens obtained from the API 5L-X52 pipe steel and (b) photograph of corrosion electrode used in this study.

All electrodes were artificially aged in a Carbolite furnace at 250 +/- 5 °C during 500 hours and 900 hours. The aged electrodes were mounted in epoxy resin to assure the exposure area (Figure 1b). Electrodes were prepared by metallographic technique, degreased with ethanol, washed with double distilled water, and hot dried before immersing in the corrosion medium. The electrodes of the weld

bead and base metal showed a transversal working area to the rolling direction, while the HAZ electrodes exhibited a longitudinal surface area along with the rolling direction due to the narrow width of this zone.

## 2.2. Electrochemical measurements

A synthetic brine (100 mL) was prepared by using analytical reagents: 9.62 g NaCl, 0.305 g CaCl<sub>2</sub>, 0.186 g MgCl<sub>2</sub>·6H<sub>2</sub>O, 0.0004 g Na<sub>2</sub>SO<sub>3</sub>, and 89.89 ml distilled water. The synthetic H<sub>2</sub>S had been generated in situ by adding 0.170 ml CH<sub>3</sub>COOH and 0.353 ml Na<sub>2</sub>S·9H<sub>2</sub>O to the brine according to NACE 1D-182 [16]. Thus, the aqueous solution of synthetic brine, initially had a concentration of hydrogen sulfide of 500 mgL<sup>-1</sup>. The H<sub>2</sub>S concentration in the solution was controlled by periodical pH measurements which were done by a buffer solution during each 10 minutes. The aforementioned brine allow to simulate an environment containing hydrogen sulfide liked to the water condense in the pipelines transporting oil. The simulant solution was purged with high purity nitrogen (2Lmin<sup>-1</sup>) before and during testing to remove oxygen from inside and over the brine.

The conventional polarisation glass cell formed by three-electrodes according to ASTM G-5 [17], included working electrodes machined from the weld bead, the complete HAZ and the base metal, a saturated Calomel reference electrode (SCE) of fixed potential of 0.2415 V, and a graphite bar as auxiliary electrode. The potentiodynamic polarisation measurements were performed using a potentiostat EG&G Princeton Applied Research model 273A controlled by a computer with PAR M352/ 252 corrosion analysis software. The electrochemical testing was carried out by polarizing the electrode approximately at ± 250 mV from the open circuit potential (OCP) using a slow scan rate of 0.166 mVs<sup>-1</sup> at room temperature of 25 °C. All the above tests were operated in static condition.

The resulting current of the polarisation tests were plotted on logarithmic scale to obtain the potentiodynamic current-potential curves for each aging condition and microstructure. The corrosion current densities,  $i_{\text{corr}}$ , were obtained by the Tafel extrapolation of the cathodic and anodic linear portions +/- 100 mV from corrosion potential ( $E_{\text{corr}}$ ). The general corrosion rate,  $V_{\text{corr}}$ , was calculated from  $i_{\text{corr}}$  by using equation (1), according to ASTM G-102 [18].

$$V_{\text{corr}} = 0.0033 (i_{\text{corr}} \text{EW} / d) \quad (1)$$

Where:

$V_{\text{corr}}$  = corrosion rate (mm y<sup>-1</sup>)

$i_{\text{corr}}$  = corrosion current density (μA cm<sup>-2</sup>)

EW = equivalent weight of the corroding species (g)

d = density of the corroding species (g cm<sup>-3</sup>)

### 2.3. Analysis of the corrosion products

After electrochemical testing, the morphological and chemical characterizations of the superficial corroding scales on the electrodes obtained from the weld bead, the HAZ and the base metal aged for 500 hours and 900 hours were carried out by means of a JEOL 6300 scanning electron microscope. The chemical composition was performed by energy dispersive X-ray spectroscopy (EDXS) using an energy dispersive spectrometer, which is attached to the microscope. The microscope was operated at 15 kV, 220  $\mu$ A, using a secondary electron detector, and working distance of 15 mm and 20 mm. The EDX spectra of the corrosion products exhibited palladium (Pd) and gold (Au) peaks. The presence of these peaks in the spectra was for the evaporation of these chemical elements on the surfaces to improve the electrical conduction and avoid the contamination of the microscope's chamber.

### 2.4. Microstructure

The microstructural and chemical characterizations of the aged weld bead, the HAZ and the base metal specimens were explored by means of a JEOL- 2000FX-II TEM transmission electron microscope operated at 200 kV and equipped with an EDX spectroscope to make the local chemical analysis of the precipitates. The thin foils of 3 mm diameter were prepared by grinding and jet-polishing to perforation, using a twin-jet electropolisher and 30 vol.% HNO<sub>3</sub>+70 vol.% CH<sub>3</sub>OH solution at -55 °C.

## 3. RESULTS AND DISCUSSION

Notable changes were observed in the corrosion behavior on the weld bead, the HAZ and the base metal thermally aged at 250 °C by 500 hours and 900 hours. These included: Tafel plots were shifted to high current density region as a function of the aging time, increase in the corrosion current densities and as a consequence a proportional increment in the general corrosion rate. This electrochemical behavior was confirmed after SEM observations on the surface of corroded specimens which revealed the corrosion products mainly iron oxide and iron sulphur with different morphology, degrees of brittleness, porosity and chemical compositions among the three different zones.

### 3.1. Potentiodynamic polarisation curves

The aged weld bead, the HAZ and the base metal showed a slight displacement to the right of the Tafel plots with the aging time which indicated a more negative corrosion potentials and increase in the demand of corrosion current. The nature of polarisation curves predicted active corrosion behavior. Similar behavior was found and reported in the literature for pipe steel API X52 and stainless steel 2101 in a chloride media [9,10]. This electrochemical behavior was more significant for the weld bead, followed by the HAZ and the base metal, see Figure 2 where clearly is observed that the cathodic

curve showed a typical linear behavior of Tafel with a slope of 100 mV for all conditions. This behavior favored the corrosion process affecting the metal surface on the specimens aged.

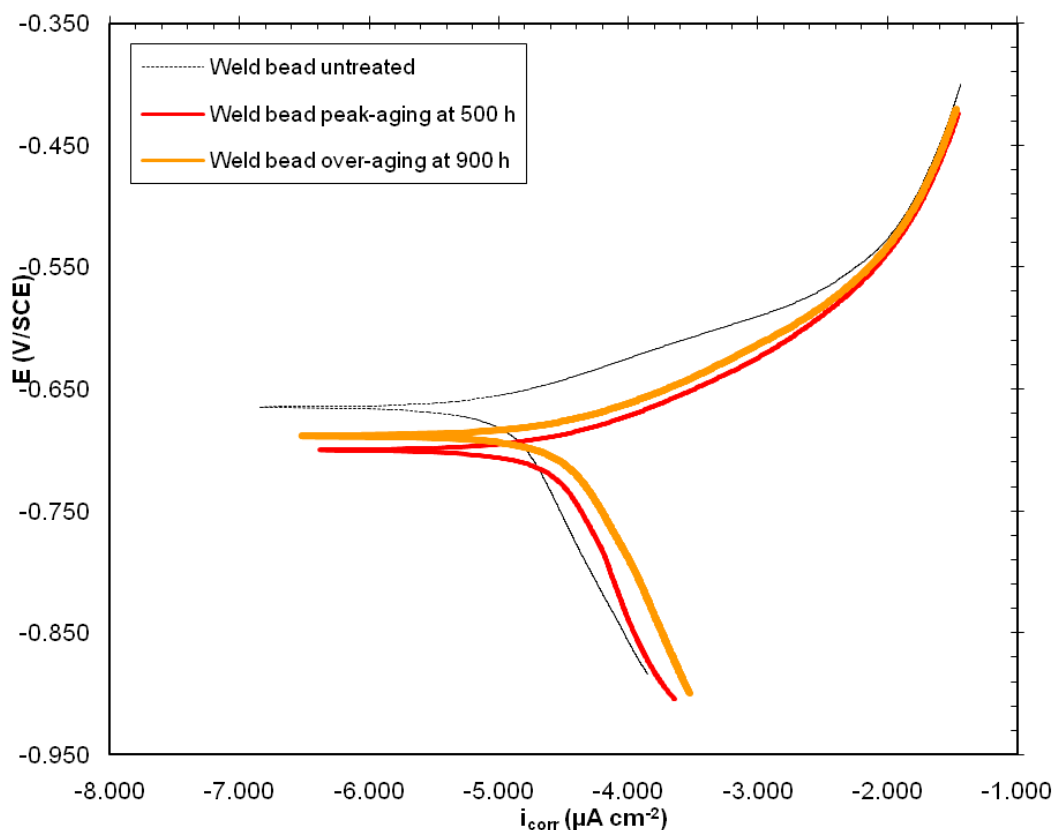


**Figure 2.** Potentiodynamic polarisation curves of weld bead specimen aged at 250 °C by 500 hours and 900 hours, tested with simulated H<sub>2</sub>S solution.

### 3.2. Tafel polarisation measurements

Results related with the electrochemical measurements indicated that the accelerated aging produced an increase in the corrosion current densities ( $i_{\text{corr}}$ ) as a function of test time [9,10] for the three different microstructural zones. The weld bead exhibited superior values of  $i_{\text{corr}}$  for 500 hours and 900 hours compared to that of the HAZ and the base metal, as can be seen in Figure 3. Also, the weld bead developed the highest increase in corrosion current density (36%) than that of the HAZ (26%) and the base metal (15%) at 900 hours of over-aging compared to the untreated condition.

The general corrosion rate ( $V_{\text{corr}}$ ) of the specimens in H<sub>2</sub>S containing brine solution had similar behavior to the corrosion current owing to the direct relationship between the corrosion rate and corrosion current developed as can be seen in the equation (1), which was derived from the Faraday law. The similar behavior between these electrochemical parameters was based on the fact that the increase in current favored the corrosion process.

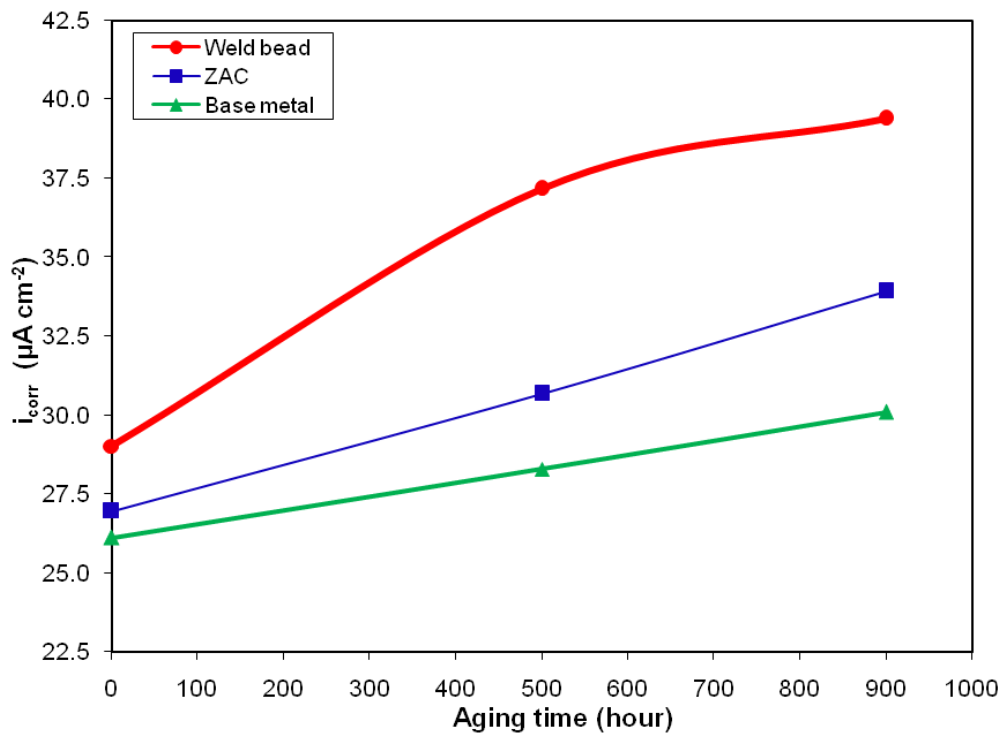


**Figure 3.** Corrosion current density as a function of aging time of welded joints aged at 250 °C by 500 hours and 900 hours, tested with simulated H<sub>2</sub>S media.

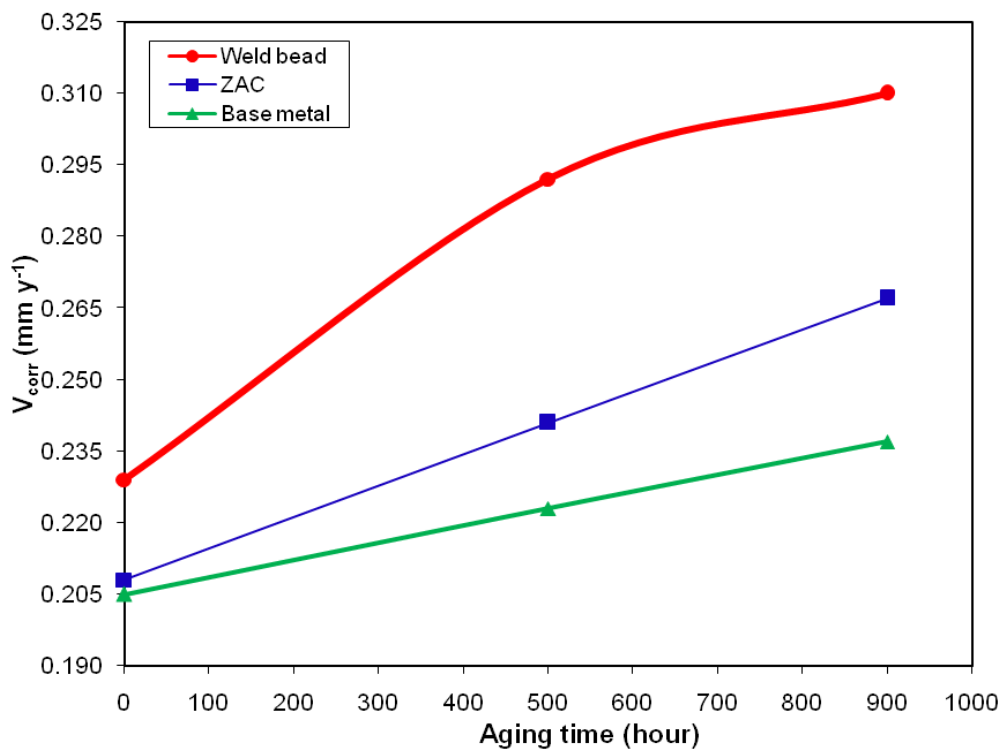


**Figure 4.** Corrosion rate vs aging time for the welded joints aged at 250 °C by 500 hours and 900 hours, tested with simulated H<sub>2</sub>S solution.

Therefore, the presence of  $H_2S$  increased the corrosion rate and became pronounced as the aging time is extended during aging treatment for the three different zones, as illustrated in Figure 4. The weld bead showed superior values of corrosion rate in all cases, followed by the HAZ and the base metal. Moreover, the weld bead reached the highest increase in rate of general corrosion (35%) than that of the HAZ (28%) and the base metal (15%) at 900 hours of over-aging, compared to that in the untreated condition. Thus, the aged weld bead became more susceptible to hydrogen sulfide corrosion process, because artificial aging may induced the development of corrosion initiation sites with different chemical composition.

### 3.3. Corrosion products

Additional indirect measurements of the electrochemical behavior of corrosion involving the increase in corrosion current densities and corrosion rate were carried out by the morphological and chemical characterizations of the superficial corroded specimens.

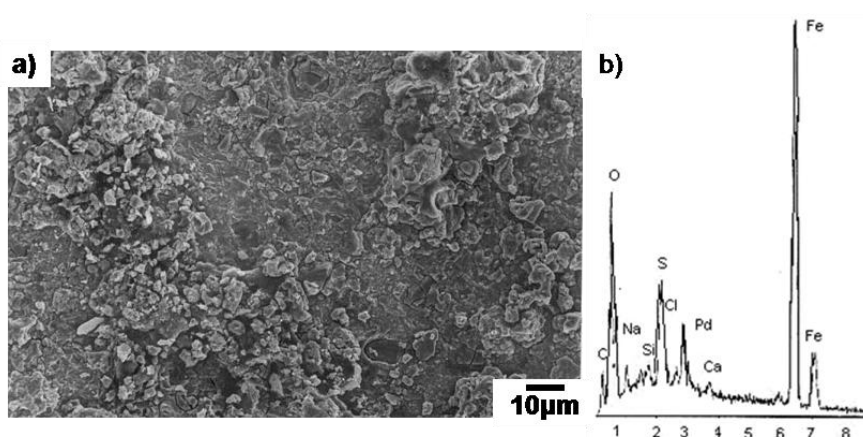


**Figure 5.** SEM image of corroded specimen for the weld bead on API 5L X52 steel over-aged by 900 hours, after testing with simulated  $H_2S$  media at 25 °C: (a) shallow brittle corrosion products, and (b) its corresponding EDX spectrum indicating Fe, S and O peaks.

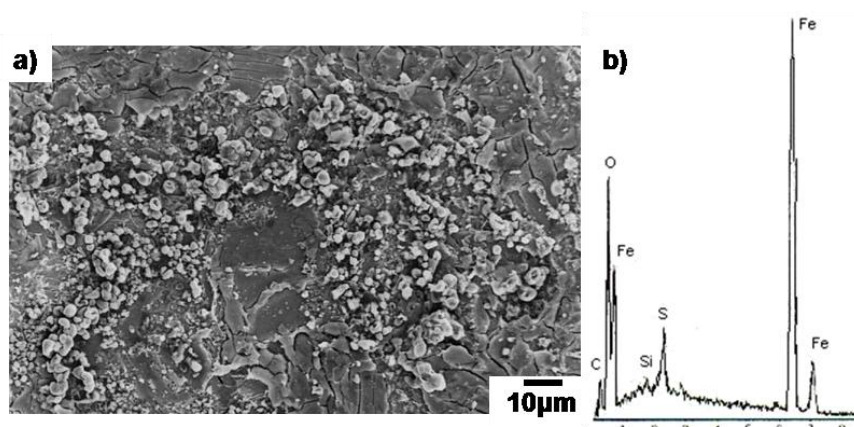


**Figure 6.** SEM images of corroded specimen for the HAZ on API 5L X52 steel over-aged by 900 hours, after testing with simulated hydrogen sulfide media at 25 °C: (a) fine brittle corrosion products, and (b) its X-ray spectrum.

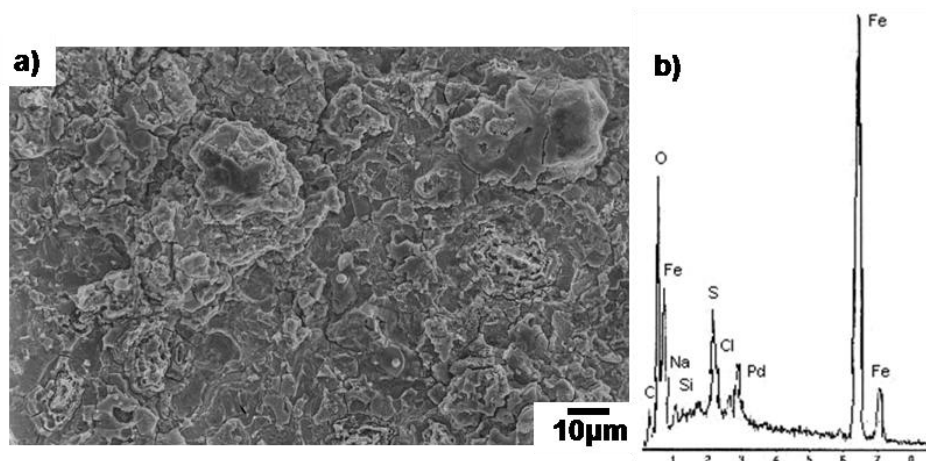


**Figure 7.** SEM image of corroded specimen for the base metal on API 5L X52 steel over-aged by 900 hours, after testing with simulated  $H_2S$  media at 25 °C: (a) gross brittle corrosion products, and (b) its EDX spectrum indicating Fe, S and O peaks.

Corrosion in a more or less uniform manner on the surface of the aged specimens was found for the weld bead, the HAZ and the base metal. Corroding surfaces exhibited the formation of corrosion products that consisted of oxide-sulphur iron as reported in the literature [6,8,19] and as indicated in the chemical elements displayed in the EDX spectra showed in Figure 5b, Figure 6b and Figure 7b. These compounds had different chemical and morphological characteristics, see SEM micrographs of same Figures.

Brittle porous corrosion products were formed on exposure area, although the products formed may be considered conductive, a thin layer of Pd and Au was deposited on these to improve the electrical conduction and avoid the contamination of the microscope. Corroded surfaces of the weld bead aged at 900 hours showed porous shallow corrosion products, see Figure 5a. The HAZ of aged sample by 900 hours presented fine corrosion products compared to the weld bead at the same condition (Figure 6a).

As can be seen, the aging process favored the formation of gross corrosion products with porosity for the base metal [9] of the specimen aged at 900 hours compared to that sample in the untreated condition, see Figure 7a. The chemical characterization of the corrosion products indicated that the composition illustrated in EDX spectrums, displayed the characteristic Fe, S and O peaks, and small peaks of Na, C, Cl and Ca for the weld bead, the HAZ and the base metal, as can be seen in Figures 5b, 6b and 7b, respectively.

Therefore, the specimen of the weld bead aged at 900 hours exhibited corrosion products with major brittleness and porosity than that of the HAZ and the base metal. This morphology of products favored the corrosion process, i.e., an increase in the corrosion current densities with the aging time, as a consequence giving increase of the general corrosion rate in hydrogen sulfide solution of the weld bead, followed by the HAZ and the base metal.

The corrosion behavior of the aged three different zones was linked to the microstructural changes that will be explained in the following section.

### 3.4. Microstructural analysis

Transmission electron microscopy (TEM) analysis performed on the aged weld bead, the HAZ, and the base metal specimens revealed the presence of transgranular nanocarbides among dislocations [20], showing notable changes in the amount, size, morphology, structure, and chemical composition as a function of aging time between the three zones, which have been published elsewhere [3,4]. The electrochemical behavior may be related with two microstructural changes.

Firstly, a precipitation [7,21] of fine nanocementite [3] during the early periods of aging process until peak-aging at 500 hours, and followed by a coarsening process of carbides [22] which was the dominant microstructural process as a consequence of the over-aging for times longer than 500 hours [4]. A TEM image of the weld bead aged at 900 hours showed medium carbides located between dislocations as shown in Figure 8a.

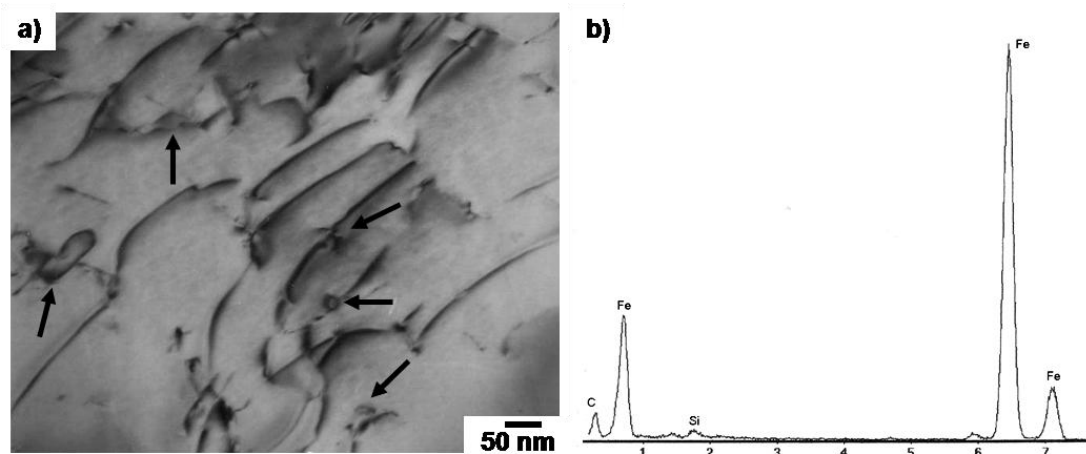


**Figure 8.** TEM bright field image obtained from the weld metal at over-aging by 900 hours: (a) coarsened medium nanoparticles located among dislocations, and (b) its corresponding EDX analysis indicating Fe and C peaks.

The X-ray spectrum displayed the Fe and C peaks, see Figure 8b. These precipitated and coarsened carbides in the three microstructural zones of the welded joint represented potential initiation sites for the corrosion process [10] in the  $H_2S$  solution.

The weld bead showed more susceptibility to corrosion process, followed by the complete HAZ and the base metal, because of the highest increase in corrosion current density (36%) and general corrosion rate (35%), and displacement to the right of the polarisation curve, which resulting in the formation of Fe-S-O containing corrosion products with brittleness and porosity after 900 hours of over-aging compared to those of the untreated condition. Moreover, the increment in the corrosion current densities could be related to the deterioration of the Charpy V-notch impact energy because of the precipitation of carbides [23] in the aged weld bead which is reported elsewhere [12]. The corrosion behavior of the aged weld bead was associated to a larger amount of corroding initiation

sites related to the largest amount of cementite precipitated at 500 hours [3] and their lower coarsening for the over-aging at 900 hours [4].

The corrosion behavior of the complete HAZ was affected by the heterogeneous microstructures produced by the welding cycle, which was modified by the thermal aging. The HAZ exhibited a medium increase in the amount of nanoparticles precipitated and a minor increment in particle size [4]. This corrosion results suggested an average rate of general corrosion with fine brittle corrosion products among the weld bead and base metal.

The electrochemical response of the base metal may be related to a lower increase in the amount of precipitated carbides and the largest increase in particle size [4] generated by the aging process, which affected the amount of initiation sites for the corrosion process giving a reduction of general corrosion rate and porous corrosion products.

#### 4. CONCLUSIONS

The susceptibility to hydrogen sulfide corrosion process of the weld bead, the complete HAZ and the base metal of the welded joint was affected by the thermal aging at 250 °C, resulting in the degradation of the corrosion resistance with the aging time. The potential corroding initiation sites were associated with the presence of transgranular nanoparticles precipitated and coarsened during the aging.

An increase in the corrosion current and rate of general corrosion was found as a function of the aging time, which was linked to the precipitation of carbides up to peak-aging at 500 hours, and to a coarsening process of these nanoparticles due to the over-aging after 500 hours.

The deterioration of the corrosion resistance was confirmed by the formation of brittle porous corrosion products of iron sulfide and iron oxide with considerable differences in the morphology for the three different microstructural zones.

The corrosion resistance of the aged weld bead was more affected by the accelerated aging than the complete HAZ and the base metal because of a higher corrosion rate, shallow corrosion products, higher increase in carbide precipitation at the peak-aging, and their lower coarsening after 500 hours.

#### ACKNOWLEDGEMENTS

The authors wish to thank the experimental and financial supports received from the Program of Development and Technology PEP-IPN and CONACYT.

#### References

1. T. Gladman, *The Physical Metallurgy of Microalloyed Steels*, The Institute of Materials, United Kingdom (1997) 185.
2. C. W. Leslie, *The Physical Metallurgy of Steels*, McGraw-Hill, Japan (1982) 79.
3. B. Vargas-Arista, A. Albiter, C. Ángeles-Chávez, and J. M Hallen, *Metall. Mater. Trans. A Phys. Metall. Mater. Sci.*, 37A (2006) 2683.

4. B. Vargas-Arista, J. M Hallen, and A. Albiter, *Mater. Charact.* 58(2007) 721.
5. F. Farelas, A. Ramirez, *Int. J. Electrochem. Sci.*, 5 (2010) 797.
6. P. R. Rhodes, *Corr. Sci.*, 57 (2001) 923.
7. T. Poornima, J. Nayak, and N. Shetty, *Int. J. Electrochem. Sci.*, 5 (2010) 56.
8. I. Hamada and K. Yamauchi, *Metall. Mater. Trans. A Phys. Metall. Mater. Sci.*, 33A (2002) 1743.
9. P. Morales-Gil, M. Romero-Romo, C. Ángeles-Chávez, and M. Palomar-Pardavé, XVIII Congreso de Sociedad Mexicana de Electroquímica. Chihuahua, México, 1 (2003) 1.
10. L. Zhang, Y. Jiang, B. Deng, W. Zhang, J. Xu, and J. Li, *Mater. Charact.*, 60 (2009) 1522.
11. K. Homma, C. Miki, H. Yang, *Engineering Fracture Mechanics*, 59 (1998) 17.
12. B. Vargas-Arista, J. M Hallen, A. Albiter, and C. Ángeles-Chávez, *Welding Int.*, 24 (2010) 315.
13. B. Vargas-Arista, C. Ángeles-Chávez, A. Albiter, and J. M Hallen, *Mater. Charact.*, 60 (2009) 1561.
14. API Standard 1104, Welding of Pipelines and Related Facilities, 20th ed., *American Petroleum Institute*, (2007) p. 2-7.
15. API Specification 5L, Specification for Line Pipe. 44th ed., *American Petroleum Institute*, (2008) p. 23-29.
16. NACE 1D-182, Wheel Test Method Used for Evaluation of Film-Persistent Corrosion Inhibitors for Oilfield Applications, (1995) p. 2.
17. ASTM Standard G-5, Standard Reference Test Method for Making Potentiostatic and Potentiodynamic Anodic Polarization Measurements, (2004) p. 71-3.
18. ASTM Standard G-102, Standard Practice for Calculation of Corrosion Rates and Related Information from Electrochemical Measurements, (2004) p.1-5.
19. Ch. Ren, D. Liu, Z. Bai, and T. Li, *Mater. Chem. Phys.*, 93 (2005) 305.
20. M. L. Saucedo-Muñoz, S. I. Komazaki, T. Hashida, T. Shoji, and V. M. López-Hirata, *Rev. Metal. Madrid*, 39 (2003) 378.
21. Z. X. Yuan, S. H. Song, Y. H. Wang, J. Liu, A. M. Guo, *Mater. Lett.*, 59 (2005) 2048.
22. J. Moon, Ch. Lee, S. Uhm, J. Lee, *Acta Mater.* 54 (2006) 1053.
23. M. L. Saucedo-Muñoz, V. M. Lopez-Hirata, E. O. Avila-Davila, D. V. Melo-Maximo, *Mater. Charact.* 60 (2009) 119.